A Geodesic Event-Study Formalism for Deep-Ocean DART Response After Large Earthquakes

Jonathan R. Landers
0000-0003-1872-6179
Independent Researcher

Abstract

Deep-ocean Assessment and Reporting of Tsunamis (DART®) stations measure bottom-pressure-derived water-column height and are designed to resolve long-period tsunami-scale ocean response in the open ocean. We formulate the relation between large earthquakes and DART® observations as a station-normalized event study. For each earthquake-station pair, great-circle distance defines an expected arrival cone; local differencing and high-pass features define comparable station response; and station-matched random windows define the null distribution. The mathematical contribution is a magnitude-geodesic cone-collapse theorem: under damped linear shallow-water propagation on the sphere, the leading event response has a common arrival-time shape after scaling by magnitude, damping, and spherical spreading, up to fixed station-feature gains. In live-feed experiments over a 45-day USGS/NDBC window, standard meteorological buoys showed no significant wave-height response, while DART® water-column histories showed elevated post-earthquake activity. The strongest result was in the theorem-derived diagnostic for M7+ events, where the 15-minute step feature gave a geometry/magnitude-scaled cone response of 0.766 against a matched-null mean of 0.394, with empirical upper-tail $p = 0.008$ from 500 station-matched randomizations.

Index Terms

DART buoys, tsunami detection, event study, matched randomization, shallow-water equations, earthquake response, geodesic scaling.

I. Introduction

Large submarine earthquakes can couple energy into the ocean column. The observational task is to measure whether deep-ocean water-column activity after an earthquake exceeds what the same stations exhibit at comparable non-event times, and whether any excess is organized by the travel-time geometry of long ocean waves. This paper turns that task into a compact event-study statistic and a falsifiable geodesic hypothesis.

The DART® observing system is the appropriate instrument class for this question. A DART® station consists of a seafloor bottom pressure recorder and a surface buoy for real-time communications; NOAA archives quality-controlled ocean bottom pressure products and identifies DART® as an open-ocean tsunami measurement system capable of detecting centimeter-scale signals [1, 2]. The NDBC real-time files used here cover the current 45-day window and provide public station histories [3]. Earthquake origin times, magnitudes, depths, and epicenters are retrieved from the USGS FDSN event service and ComCat [4, 5].

The contribution is threefold. First, we define a station-local response statistic that compares post-earthquake windows against matched random windows from the same station history. Second, we prove a cone-collapse statement showing why a water-column response should align in the coordinate $\xi = (t - t_i - D_{\mathrm{gc}}(x_i, y_j)/c)/\omega$, after spherical spreading and magnitude scaling. Third, we report experiments showing a clean separation between standard NDBC meteorological buoys and DART® bottom-pressure-derived water-column histories. The resulting diagnostic connects an interpretable statistical design to the geometry used in tsunami propagation and forecasting.

II. Background and Positioning

Operational tsunami forecasting combines fast earthquake characterization, precomputed or rapid propagation models, and offshore observations. The DART® program and the NTHMP tsunameter network established the value of direct deep-ocean measurements [6–9]. NOAA's SIFT propagation database uses linear combinations of precomputed unit-source simulations, with DART® inversions used to refine forecasts as waves reach offshore instruments [10, 11]. Recent probabilistic workflows similarly update tsunami forecasts as seismic and ocean observations arrive [12, 13].

This work targets a complementary layer: a network-level test for anomalous post-event DART® response after conditioning on station identity. The statistical side follows the spirit of earthquake point-process work: Gutenberg-Richter magnitude-frequency scaling, energy-magnitude scaling, ETAS-style clustering, and unified waiting-time laws all show that earthquake catalogs contain strong nonstationarity and clustering [14–17]. Matching null windows within the same station history is a pragmatic way to preserve local tides, telemetry cadence, and instrument variance while isolating the event-time contrast.

The wave side is deliberately first order. Long tsunami waves are commonly approximated with shallow-water dynamics, and operational propagation models exploit near-linearity offshore [10, 18, 19]. Recent work has emphasized that global-scale propagation benefits from spherical geometry, including focusing and defocusing away from local Cartesian approximations [20, 21]. This motivates a geodesic arrival coordinate rather than an unaligned 0–24 h post-event average alone.

III. Event-Study Formalism

Let the earthquake catalog be

$$\mathcal{Q} = \{q_i = (t_i, x_i, M_i, d_i)\}_{i=1}^{n}, \tag{1}$$

where t_i is origin time, x_i epicentral position, M_i magnitude, and d_i depth. Let the DART® network be $\mathcal{B} = \{b_j = (y_j)\}_{j=1}^{m}$, with station position y_j and water-column height $H_j(t)$. For a quake-station pair,

$$r_{ij} = D_{\mathrm{gc}}(x_i, y_j), \qquad \tau_{ij} = r_{ij}/c, \qquad c = 750 \text{ km h}^{-1}, \tag{2}$$

where c is a rough open-ocean tsunami speed proxy used only to align windows.

Two station-local features were used. A short-step feature emphasizes abrupt changes:

$$S_j(t) = H_j(t) - H_j(t - \delta), \qquad \delta = 15 \text{ min}. \tag{3}$$

A high-pass feature removes slow background structure:

$$A_j(t) = H_j(t) - \frac{1}{|K(t)|} \sum_{u \in K(t)} H_j(u), \qquad K(t) = \{u : |u - t| \le 12 \text{ h}\}. \tag{4}$$

For $m \in \{S, A\}$, station standardization gives

$$Z_j^{(m)}(t) = \frac{m_j(t) - \mu_j^{(m)}}{\sigma_j^{(m)}}. \tag{5}$$

The event window is either the broad post-event interval $[t_i, t_i + 24 \text{ h}]$ or an arrival window around τ_{ij}:

$$W_{ij}^{+} = [t_i + \max(0, \tau_{ij} - \eta_-),\ t_i + \tau_{ij} + \eta_+], \tag{6}$$

with $\eta_- = 2$ h and $\eta_+ = 8$ h in the DART® experiment. The pre-event comparison is $W_{ij}^{-} = [t_i - 24 \text{ h}, t_i]$. Pair-level response is

$$R_{ij}^{(m)} = \max_{t \in W_{ij}^{+}} |Z_j^{(m)}(t)|, \qquad \Delta R_{ij}^{(m)} = R_{ij}^{(m)} - \max_{t \in W_{ij}^{-}} |Z_j^{(m)}(t)|. \tag{7}$$

For a filtered pair set $\mathcal{P}$, aggregate statistics are

$$T_m = \frac{1}{|\mathcal{P}|} \sum_{(i,j) \in \mathcal{P}} R_{ij}^{(m)}, \qquad U_{m,\kappa} = \frac{1}{|\mathcal{P}|} \sum_{(i,j) \in \mathcal{P}} \mathbf{1}\{R_{ij}^{(m)} \ge \kappa\}. \tag{8}$$

The null samples random matched times $u_{ij}^{(b)}$ from the same station history, applies the same window geometry, and recomputes the statistic. The empirical upper-tail value is

$$\widehat{p} = \frac{1 + \sum_{b=1}^{B} \mathbf{1}\{T_m^{(b)} \ge T_m\}}{B + 1}, \tag{9}$$

with $B = 500$ for the DART® runs.

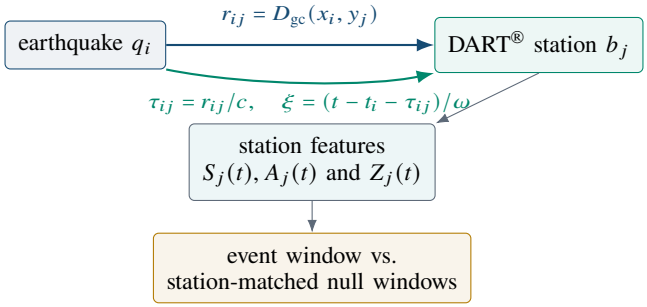

Fig. 1. The statistic aligns each earthquake-station pair by geodesic arrival time, computes station-normalized water-column activity, and compares the event window with random windows from the same station.

IV. Cone-Collapse Theorem

The event statistic above becomes sharper when the response is expressed in the natural travel-time coordinate. The theorem below states the reason: for offshore long waves on a sphere, the leading earthquake-generated height field separates into a source-amplitude factor, a damping factor, a spherical spreading factor, and a common arrival waveform.

Theorem 1 (Magnitude-geodesic collapse of DART® response): Let the open-ocean height perturbation η satisfy a damped linear shallow-water equation on a sphere S_R^2, away from coastlines, the source point, and antipodal caustics:

$$\left(\partial_t^2 + 2\gamma\partial_t - c^2\Delta_{S_R^2}\right)\eta(x,t) = \sum_i A_i\psi_i(t-t_i)\delta_{x_i}(x), \qquad A_i = A_0\, 10^{0.75(M_i - M_0)}. \tag{10}$$

Assume the source pulses share a normalized shape, $\psi_i(s) = \omega^{-1}\psi(s/\omega) + O(\varepsilon_{\mathrm{src}})$, and that a DART® record can be written locally as

$$H_j(t) = B_j(t) + g_j\eta(y_j,t) + \nu_j(t), \tag{11}$$

where B_j and ν_j have zero conditional event-time mean after station-local matching. Let L_m be any linear time-invariant feature operator, including the step and high-pass operators above, and let

$$Z_j^{(m)}(t) = \frac{L_m H_j(t) - \mu_j^{(m)}}{\sigma_j^{(m)}}. \tag{12}$$

Define $\theta_{ij} = D_{\mathrm{gc}}(x_i, y_j)/R$, $\tau_{ij} = R\theta_{ij}/c$, and $\xi_{ij}(t) = (t - t_i - \tau_{ij})/\omega$. Then the collapsed response

$$\widetilde{Z}_{ij}^{(m)}(\xi) = 10^{-0.75(M_i - M_0)}\, e^{\gamma\tau_{ij}}\sqrt{\sin\theta_{ij}}\, Z_j^{(m)}(t_i + \tau_{ij} + \omega\xi). \tag{13}$$

satisfies

$$\mathbb{E}\left[\widetilde{Z}_{ij}^{(m)}(\xi) \mid q_i, y_j\right] = \rho_j^{(m)} K_m(\xi) + O(\varepsilon_{\mathrm{bath}} + \varepsilon_{\mathrm{coast}} + \varepsilon_{\mathrm{src}} + \varepsilon_{\mathrm{noise}}), \tag{14}$$

where $\rho_j^{(m)} = A_0 g_j/\sigma_j^{(m)}$ is fixed for a station-feature pair, and K_m depends on the feature and source pulse family but not on earthquake magnitude, distance, or origin time.

Proof. By linearity, the contribution of earthquake q_i at station y_j is

$$\eta_i(y_j,t) = A_i \int G_\gamma(y_j, t; x_i, t_i + s)\psi_i(s)\, ds, \tag{15}$$

where G_γ is the retarded Green function for the damped spherical wave operator. For $0 < \theta_{ij} < \pi$, and away from shoreline and bathymetric scattering, the Hadamard–geometric-optics parametrix for the spherical wave kernel gives

$$G_\gamma(y_j, t; x_i, t_i) = e^{-\gamma(t-t_i)} a_0 (\sin\theta_{ij})^{-1/2}\mathcal{G}\left(t - t_i - \tau_{ij}\right) + E_{ij}(t), \tag{16}$$

where the Van Vleck determinant on S_R^2 supplies the $(\sin\theta_{ij})^{-1/2}$ spreading factor, $\tau_{ij} = R\theta_{ij}/c$, and E_{ij} collects bathymetric, coastal, caustic, and finite-bandwidth errors. Convolving (16) with the normalized source pulse and evaluating at $t = t_i + \tau_{ij} + \omega\xi$ yields

$$\eta_i(y_j, t_i + \tau_{ij} + \omega\xi) = A_i e^{-\gamma\tau_{ij}} (\sin\theta_{ij})^{-1/2} h(\xi) + O(\varepsilon_{\text{bath}} + \varepsilon_{\text{coast}} + \varepsilon_{\text{src}}), \tag{17}$$

with h determined only by ψ, $\mathcal{G}$, and the nondimensional window coordinate. The factor $e^{-\gamma\omega\xi}$ over the local arrival window is absorbed into h when γ is fixed, and into the residual when it is estimated coarsely.

Apply the linear time-invariant feature L_m. Because L_m commutes with time translation and convolution,

$$L_m\eta_i(y_j, t_i + \tau_{ij} + \omega\xi) = A_i e^{-\gamma\tau_{ij}} (\sin\theta_{ij})^{-1/2} K_m(\xi) + O(\varepsilon_{\text{bath}} + \varepsilon_{\text{coast}} + \varepsilon_{\text{src}}), \tag{18}$$

where $K_m = L_m h$ in the arrival coordinate. The observation equation gives

$$\mathbb{E}\big[L_m H_j(t_i + \tau_{ij} + \omega\xi) \mid q_i, y_j\big] = g_j A_i e^{-\gamma\tau_{ij}} (\sin\theta_{ij})^{-1/2} K_m(\xi) + O(\varepsilon_{\text{bath}} + \varepsilon_{\text{coast}} + \varepsilon_{\text{src}} + \varepsilon_{\text{noise}}), \tag{19}$$

because the matched station background and sensor noise have zero conditional event-time mean. Subtracting the station mean and dividing by $\sigma_j^{(m)}$ therefore gives

$$\mathbb{E}\left[Z_j^{(m)}(t_i + \tau_{ij} + \omega\xi) \mid q_i, y_j\right] = \frac{g_j A_i}{\sigma_j^{(m)}} e^{-\gamma\tau_{ij}} (\sin\theta_{ij})^{-1/2} K_m(\xi) + O(\varepsilon_{\text{bath}} + \varepsilon_{\text{coast}} + \varepsilon_{\text{src}} + \varepsilon_{\text{noise}}). \tag{20}$$

Multiplying by the collapse factor in (13) and substituting $A_i = A_0\, 10^{0.75(M_i - M_0)}$ proves (14). ∎

The theorem yields two empirical diagnostics. The first asks whether strong standardized response lies near $\xi = 0$; the second asks whether the magnitude- and geometry-scaled cone mean exceeds matched station histories. Let t_{ij}^* denote the time attaining the pairwise maximum in the evaluated cone. With $\gamma = 0$ in the reported experiments,

$$C_m = \Pr\{|Z_j^{(m)}(t_{ij}^*)| \geq 3,\ |\xi_{ij}(t_{ij}^*)| \leq 1\}, \tag{21}$$

$$G_m = \frac{1}{|\mathcal{P}|} \sum_{(i,j)} 10^{-0.75(M_i - M_0)} \sqrt{\sin\theta_{ij}} \max_{|\xi|\leq 1} |Z_j^{(m)}(t_i + \tau_{ij} + \omega\xi)|, \tag{22}$$

with $\omega = 3$ h. The station-matched randomization tests whether C_m and G_m exceed the same quantities computed at non-event times from the same instruments.

V. Experiments

The experiments were run over the same recent 45-day USGS/NDBC live-feed window. Standard NDBC station histories were first tested to establish the instrument contrast. Then DART® water-column histories were tested at M6.5+ and M7+ thresholds. Candidate station pairs were distance-filtered and then pruned to station histories with usable data. Null distributions used 500 random matched windows for the DART® runs and the same window definitions as the observed statistic.

Figure 1 shows the pipeline. Figure 2 shows that the DART® M6.5+ experiment produced elevated observed response relative to matched station-local null means in both broad post-event and arrival windows. Figure 3 shows that the theorem-derived cone statistics remain below the 0.05 line, with strongest evidence in cone-pre delta and scaled cone mean. Table I summarizes all reported runs.

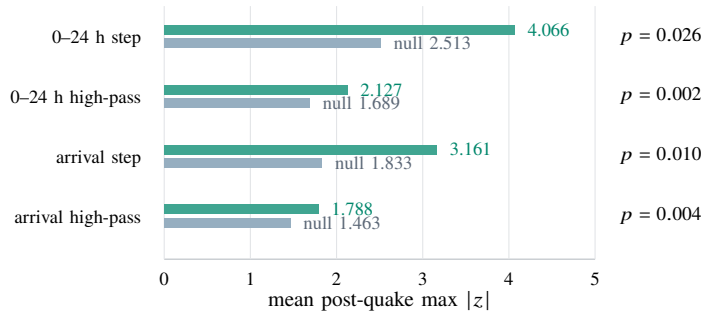

Fig. 2. DART® M6.5+ experiment with 7 earthquakes and 41 usable quake-DART pairs. Green bars are observed event windows; blue bars are matched-window null means from the same stations.

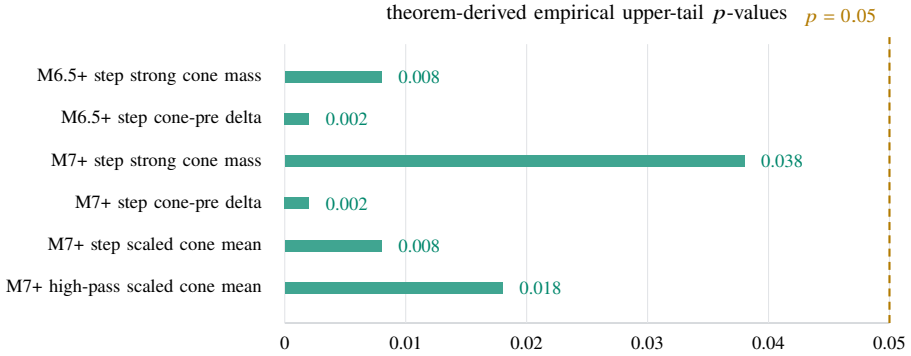

Fig. 3. Cone-collapse diagnostics using $\xi = (t - t_i - r/c)/3$ h and the spherical/magnitude scale in (22). All displayed statistics clear a 0.05 empirical threshold under station-matched randomization.

TABLE I
SUMMARY OF EXPERIMENTS REPORTED FROM THE 45-DAY LIVE-FEED SNAPSHOT.

Experiment	Data and pairing	Primary result
Standard NDBC buoys	M5.5+; 60 earthquakes; 69 candidate quake-station pairs; 54 usable history pairs	Wave height did not pass 0.05: $p = 0.213$ for 0–24 h windows and $p = 0.442$ for arrival windows.
DART® M6.5+	7 earthquakes; 48 DART® stations with files; 41 usable quake-DART® pairs	Water-column response was elevated: 15-minute step $p = 0.026$ and high-pass $p = 0.002$ in 0–24 h windows.
DART® M7+	4 earthquakes; 24 usable quake-DART® pairs	Signal strengthened: 0–24 h step $p = 0.004$; arrival-window step $p = 0.002$.
Cone collapse, M6.5+	$\xi = (t - t_i - r/c)/3$ h; 41 usable quake-DART® pairs; 500 randomizations	Step strong cone mass was 0.103 vs. null 0.036, $p = 0.008$; cone-pre delta was 0.944 vs. null -0.870, $p = 0.002$.
Cone collapse, M7+	24 usable quake-DART® pairs; M7+ threshold	Using scale $\sqrt{\sin(r/R)}10^{-0.75(M-M_0)}$, step cone mean was 0.766 vs. null 0.394, $p = 0.008$; high-pass was 0.398 vs. null 0.332, $p = 0.018$.

VI. Interpretation and Limitations

The result is intuitive: standard meteorological buoy variables are not designed to resolve deep-ocean tsunami-scale bottom pressure perturbations, while DART® water-column histories are. The observed contrast between standard buoys and DART® histories is therefore consistent with instrument physics and NOAA's operational role for DART® systems [2, 22]. The cone-collapse results are also consistent with global propagation theory: once the event is projected into geodesic arrival coordinates and scaled for magnitude and spherical spreading, excess response concentrates near $\xi = 0$ [20, 21].

Several limitations matter. The sample is small because only large recent earthquakes and usable DART® histories enter the paired design. The arrival speed in (2) is a constant proxy rather than a bathymetry-dependent travel-time model. The theorem is intentionally offshore and first order; coastlines, caustics, bathymetric refraction, source directivity, and event-mode telemetry all enter the error terms. Finally, empirical p-values are reported for multiple related diagnostics, so they should be read as evidence for a coherent pattern rather than as isolated discovery claims.

VII. Conclusion

Station-normalized DART® features, matched station-local null windows, and the geodesic cone-collapse theorem give a coherent event-study view of deep-ocean response after large earthquakes. The experiments show elevated DART® water-column activity relative to matched non-event times, while standard buoy wave-height fields do not show comparable evidence. The strongest signal appears near the expected geodesic arrival cone after physically motivated magnitude and spherical spreading normalization.

Data and Reproducibility

The experiments use public USGS event queries and NOAA/NDBC real-time station files. The implementation described here is reflected in the repository's buoy and DART® earthquake-response experiment scripts. Because the NDBC real-time directory is a moving 45-day window, exact reproduction requires archiving the queried station files and event catalog snapshot.

References

[1] National Oceanic and Atmospheric Administration, "Deep-Ocean Assessment and Reporting of Tsunamis (DART(R))," NOAA National Centers for Environmental Information, 2005, accessed 2026-04-30. [Online]. Available: https://doi.org/10.7289/V5F18WNS

[2] NOAA Center for Tsunami Research, "DART System Overview," Pacific Marine Environmental Laboratory, 2026, accessed 2026-04-30. [Online]. Available: https://nctr.pmel.noaa.gov/Dart/dart_overview.html

[3] National Data Buoy Center, "How can realtime data be retrieved from the NDBC web site?" National Oceanic and Atmospheric Administration, 2026, accessed 2026-04-30. [Online]. Available: https://www.ndbc.noaa.gov/faq/rt_data_access.shtml

[4] U.S. Geological Survey, "API Documentation: Earthquake Catalog," FDSN Event Web Service, 2026, accessed 2026-04-30. [Online]. Available: https://earthquake.usgs.gov/fdsnws/event/1/

[5] ——, "ANSS Comprehensive Earthquake Catalog (ComCat) Documentation," Earthquake Hazards Program, 2026, accessed 2026-04-30. [Online]. Available: https://www.usgs.gov/programs/earthquake-hazards/anss-comprehensive-earthquake-catalog-comcat-documentation

[6] F. I. Gonzalez, E. N. Bernard, C. Meinig, M. Eble, H. O. Mofjeld, and S. Stalin, "The nthmp tsunameter network," *Natural Hazards*, vol. 35, pp. 25–39, 2005.

[7] C. Meinig, S. E. Stalin, A. I. Nakamura, and H. B. Milburn, "Real-time deep-ocean tsunami measuring, monitoring, and reporting system: The noaa dart ii description and disclosure," NOAA Pacific Marine Environmental Laboratory, Tech. Rep., 2005. [Online]. Available: https://www.ndbc.noaa.gov/dart/dart_ii_description_6_4_05.pdf

[8] E. N. Bernard and C. Meinig, "History and future of deep-ocean tsunami measurements," in *OCEANS'11 MTS/IEEE KONA*. IEEE, 2011, pp. 1–7.

[9] G. Mungov, M. Eble, and R. Bouchard, "Dart tsunameter retrospective and real-time data: A reflection on 10 years of processing in support of tsunami research and operations," *Pure and Applied Geophysics*, vol. 170, no. 9–10, pp. 1369–1384, 2013.

[10] E. Gica, M. C. Spillane, V. V. Titov, C. D. Chamberlin, and J. C. Newman, "Development of the forecast propagation database for noaa's short-term inundation forecast for tsunamis (sift)," NOAA Pacific Marine Environmental Laboratory, Tech. Rep. NOAA Technical Memorandum OAR PMEL-139, 2008. [Online]. Available: https://repository.library.noaa.gov/view/noaa/11079

[11] NOAA Center for Tsunami Research, "Forecast Propagation Database," Pacific Marine Environmental Laboratory, 2026, accessed 2026-04-30. [Online]. Available: https://nctr.pmel.noaa.gov/propagation-database.html
[12] J. Selva *et al.*, "Probabilistic tsunami forecasting for early warning," *Nature Communications*, vol. 12, p. 5677, 2021.
[13] L. Cordrie, J. Selva, F. Bernardi, R. Tonini, F. Romano, M. Volpe, and S. Lorito, "Dynamic management of uncertainty in rapid tsunami forecasting," *Communications Earth & Environment*, vol. 6, p. 637, 2025.
[14] B. Gutenberg and C. F. Richter, "Frequency of earthquakes in california," *Bulletin of the Seismological Society of America*, vol. 34, pp. 185–188, 1944.
[15] H. Kanamori, "The energy release in great earthquakes," *Journal of Geophysical Research*, vol. 82, no. 20, pp. 2981–2987, 1977.
[16] Y. Ogata, "Statistical models for earthquake occurrences and residual analysis for point processes," *Journal of the American Statistical Association*, vol. 83, no. 401, pp. 9–27, 1988.
[17] P. Bak, K. Christensen, L. Danon, and T. Scanlon, "Unified scaling law for earthquakes," *Physical Review Letters*, vol. 88, no. 17, p. 178501, 2002.
[18] V. V. Titov and C. E. Synolakis, "Numerical modeling of tidal wave runup," *Journal of Waterway, Port, Coastal, and Ocean Engineering*, vol. 124, no. 4, pp. 157–171, 1998.
[19] D. B. Percival, D. W. Denbo, M. C. Eble, E. Gica, H. O. Mofjeld, M. C. Spillane, L. Tang, and V. V. Titov, "Extraction of tsunami source coefficients via inversion of dart buoy data," *Natural Hazards*, vol. 58, no. 1, pp. 567–590, 2011.
[20] B. Williams, A. Abdolali, and U. Kadri, "Linear propagation of tsunami and acoustic-gravity waves on a sphere: Geometrical focusing and defocusing," *Wave Motion*, vol. 140, p. 103643, 2026.
[21] A. Abdolali, M.-A. Y. Lam, U. Kadri, M. Malej, M. Filimonov, and F. Shi, "Basin-scale geometric focusing: A probabilistic-geometric framework for global tsunami hazard assessment and the 2025 kamchatka peninsula tsunami," EGUsphere preprint, 2026. [Online]. Available: https://doi.org/10.5194/egusphere-2025-6048
[22] National Data Buoy Center, "Deep-ocean Assessment and Reporting of Tsunamis (DART): Bottom Package," National Oceanic and Atmospheric Administration, 2026, accessed 2026-04-30. [Online]. Available: https://www.ndbc.noaa.gov/dart/bottom.shtml